Int. J. Heat Mass Transfer. Vol. 31, No. 4, pp. 709–722, 1988
Printed in Great Britain

0017–9310/88 $3.00 + 0.00

Analytical and experimental study of steady-state convection in a double-loop thermosyphon

MIHIR SEN,† D. A. PRUZAN and K. E. TORRANCE
Sibley School of Mechanical and Aerospace Engineering, Cornell University, Ithaca, NY 14853, U.S.A.

(*Received* 13 *January* 1987 *and in final form* 15 *July* 1987)

Abstract—Steady-state natural convection in a toroidal loop with a heated diametrical branch and cooled side branches is studied. The loop is rotated to vary the tilt angle of the diametral branch. A one-dimensional analysis provides the fluid velocities and temperature distributions in the loop. The effects of axial conduction are examined. With increasing tilt from the vertical, the fluid in the lower side branch slows down and reverses. The flow through the central branch increases and the main return path is through the upper side branch. For small tilt angles around the horizontal, multiple steady states exist. Comparison experiments on a water-filled glass loop are in qualitative agreement with the analysis and multiple steady states are observed.

INTRODUCTION

THE STEADY and time dependent behavior of closed natural circulation loops is important for engineering applications, and for an understanding of flow processes in thermosyphons. Recent advances have been reviewed [1, 2]. Many of these studies have considered loops in which a single flow channel describes a spatial configuration which closes upon itself. Most analyses have assumed one-dimensional channel flows, such that pressure, velocity and temperature are uniform over any cross-section of a channel. Qualitatively, one-dimensional models have been able to describe some of the important aspects of thermosyphon behavior. However, multi-dimensional flows do exist [3–5], and are important for the determination of friction factors and heat transfer coefficients.

Both single- and multiple-loop thermosyphons are important in practical applications. For example, the emergency cooling of a nuclear reactor might employ multiple flow paths through the reactor core [6], or the solar energy collectors for a solar power plant might be placed in parallel and be driven by natural convection. One of the early studies of multiple loops was that of Chato [7], who examined flows in a parallel-channel system and observed multiple steady states. Zvirin *et al.* [8, 9] developed a non-heat-conducting model for a loop with a single heater and multiple cooling paths. Zvirin [10] also studied the onset of motion in an arrangement of vertical tubes running between a lower heat source and an upper heat sink, and the transient behavior of loops with parallel channels [11].

There are important differences in the one-dimensional modeling of thermosyphons with single and multiple loops. This has been discussed in ref. [12] for a general configuration of tubes of arbitrary shape starting from one point and ending at another. For single loops, either axially heat-conducting or axially non-heat-conducting energy equations can be used. Axial conduction is important mainly in the study of the onset of convective motion [13], but appears to make little difference in velocity predictions. For multiple loops, however, unless all branches but one are identically equal in all respects, continuity of temperature at the branch junctions cannot be assured when axial conduction is neglected. At branch junctions, fluid streams of different temperatures may join and mix. Only an axially heat-conducting model is strictly valid, even though axial conduction might be orders of magnitude smaller than convection over most of the loop. Thus, the one-dimensional problem becomes one of singular perturbation. Thermal adjustment regions, or axial thermal boundary layers, must be included near branch junctions. Such axial boundary layers separate the flow into conducting and non-conducting, inner and outer regions, respectively [14]. The axial boundary layers should not be confused with wall boundary layers which do not arise in a one-dimensional analysis.

Another important aspect of multiple-loop thermosyphons is related to differences between branches which were designed to be identical. Manufacturing imperfections and operation over a long time can lead to slight differences in the friction, heat transfer, or geometrical characteristics. It is important to know if such differences could significantly alter the steady-state behavior. The easiest difference to introduce and measure is a change in the gravity component due to a tilt from perfect symmetry.

To examine the effect of differences between the branches of a multiple-loop thermosyphon, we will consider a toroidal loop with an extra diametral branch in the center as shown schematically in Fig. 1. This is a double-loop configuration which will permit

† Present address: Department of Aerospace and Mechanical Engineering, University of Notre Dame, Notre Dame, IN 46556, U.S.A.

NOMENCLATURE

δB	change in local buoyancy force
c	fluid specific heat
d	tube diameter
F	friction coefficient
g	acceleration due to gravity
$h(x_i^*)$	distribution of convective heat transfer coefficient, equation (6)
$H(x_i)$	non-dimensional h, equation (13)
h_0	convective heat transfer coefficient in heat exchanger
H_0	non-dimensional heat transfer coefficient in heat exchanger, equation (15a)
k	thermal conductivity
p	pressure
P	non-dimensional parameter, equation (8c)
P^*	dimensional pressure parameter, equation (4)
q'	heat input per unit length in the heater
q_h	total heat generated by electrical resistance heater
Q	non-dimensional heat input, equation (15c)
R	radius of torus
$T_i(x_i)$	non-dimensional fluid temperature in branch i, equation (8d)
$T_i^*(x_i^*)$	dimensional fluid temperature in branch i
T_0^*	reference temperature taken to be that of the cooling water
δT_i	temperature difference over the middle third of branch i
ΔT	characteristic temperature difference, equation (8e)
x_i	non-dimensional axial coordinate measured from point A, equation (8a)
x_i^*	dimensional axial coordinate measured from point A in Fig. 1
u_i	non-dimensional fluid velocity in branch i, equation (8b)
u_i^*	dimensional fluid velocity in branch i.

Greek symbols

α	tilt angle of central branch from vertical, see Fig. 1
β	volumetric thermal expansion coefficient
λ	non-dimensional axial heat conduction parameter, equation (15b)
ν	kinematic viscosity
ρ	fluid density.

Subscripts

A	upper branch junction of loop in Fig. 1
B	lower branch junction of loop in Fig. 1
i	1, 2 and 3 for right side, central and left side branches of the loop in Fig. 1.

one-dimensional analysis and a qualitative comparison with experiment. The loop can be tilted in a vertical plane. A spatially uniform heat flux is applied in the central branch. The middle thirds of the two side branches are cooled by constant temperature heat exchangers. The remaining two thirds of the side branches are adiabatic. Tilting the loop varies the angle of the diametral branch and the relative heights of the two cooling sections. In this paper, the fluid velocities and temperatures in the three branches are examined analytically and experimentally as a function of tilt angle and heat input. The role of axial conduction is also explored.

In the following sections, the non-dimensional governing equations will first be developed, followed by a discussion of branch junction conditions which apply for axially heat-conducting and axially non-heat-conducting models. Analytical and experimental results are then presented.

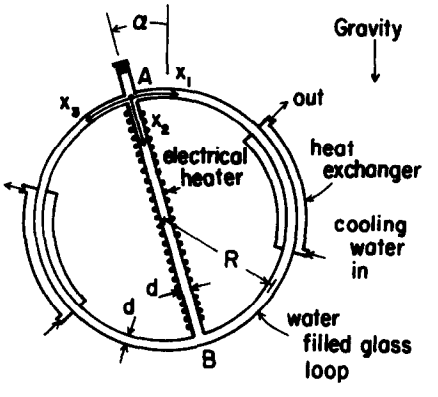

FIG. 1. Schematic of double-loop thermosyphon.

GOVERNING EQUATIONS

The branch junction A in Fig. 1 is taken to be the origin of coordinates x_i^* $(i = 1, 2, 3)$ which run along the three branches as shown. Asterisks denote the dimensional form of variables which will later be made nondimensional. Index 2 refers to the central branch and 1 and 3 to the right and left side branches, respectively. The fluid velocity u_i^* in each branch is taken as positive when directed away from A and is uniform in the axial direction, since the tubes are assumed to be of constant inside diameter d and the fluid is assumed incompressible. The radius of the outer loop is R. $T_i^*(x_i^*)$ denotes the fluid temperature in each leg

($i = 1, 2, 3$). The tilt angle α of the central branch is measured counterclockwise from the vertical. The gravity vector is vertical.

Dimensional equations

The governing one-dimensional equations in steady-state form are given in ref. [12]. From mass conservation we have

$$u_1^* + u_2^* + u_3^* = 0. \tag{1}$$

The momentum equation can be integrated along the length of each branch. For the side branches

$$\pi R F u_i^* + g\beta \int_0^{\pi R} T_i^* \sin\left(\frac{x_i^*}{R} \pm \alpha\right) \mathrm{d}x_i^* = P^*, \quad i = 1, 3 \tag{2}$$

where the negative and positive signs are for $i = 1$ and 3, respectively, and F is a friction coefficient,† g is the acceleration due to gravity, and β is the volumetric expansion coefficient. For the central branch, integration of the momentum equation yields

$$2RFu_2^* + g\beta \cos\alpha \int_0^{2R} T_2^* \, \mathrm{d}x_2^* = P^*. \tag{3}$$

The right-hand sides of equations (2) and (3) introduce a parameter, P^*, given by

$$P^* = \frac{1}{\rho}(p_A - p_B) + 2gR(1 + \beta T_0^*)\cos\alpha \tag{4}$$

where p_A and p_B are the fluid pressures at A and B and ρ is the fluid density at a reference temperature T_0^*, taken to be that of the cooling water in the heat exchangers. The product ρP^* represents the driving pressure difference for the three branches of the loop, and is equal to the pressure difference $(p_A - p_B)$ less that induced hydrostatically by the fluid at the reference temperature.

The energy equation for the side branches is

$$\frac{\pi d^2}{4}\rho c u_i^* \frac{\mathrm{d}T_i^*}{\mathrm{d}x_i^*} = \pi d h(x_i^*)(T_0^* - T_i^*) + \frac{\pi d^2}{4} k \frac{\mathrm{d}^2 T_i^*}{\mathrm{d}x_i^{*2}}, \quad i = 1, 3 \tag{5}$$

where c is the fluid specific heat, h is the convective heat transfer coefficient, and k is the fluid thermal conductivity. The wall heat transfer coefficient in equation (5) is given by

$$h(x_i^*) = \begin{cases} h_0 \text{ in } \dfrac{\pi R}{3} < x_i^* < \dfrac{2\pi R}{3} \\ 0 \text{ otherwise.} \end{cases} \tag{6}$$

The choice $h(x_i^*) = 0$ in equation (6) corresponds to the adiabatic sections of the side branches. The driving temperature difference in the heat exchangers is $(T_0^* - T_i^*)$. For the central branch

$$\frac{\pi d^2}{4}\rho c u_2^* \frac{\mathrm{d}T_2^*}{\mathrm{d}x_2^*} = q' + \frac{\pi d^2}{4} k \frac{\mathrm{d}^2 T_2^*}{\mathrm{d}x_2^{*2}} \tag{7}$$

where the heat input q' per unit length is assumed constant over the length of the branch. The last term in equations (5) and (7) represents heat transfer due to axial conduction.

Non-dimensional equations

We choose the following non-dimensional variables

$$x_i = x_i^*/\pi R \tag{8a}$$

$$u_i = u_i^*/\pi RF \tag{8b}$$

$$P = \left[\frac{1}{\rho}(p_A - p_B) + 2gR\cos\alpha\right] \Big/ \pi^2 R^2 F^2 \tag{8c}$$

$$T_i = (T_i^* - T_0^*)/\Delta T \tag{8d}$$

with

$$\Delta T = \pi RF^2/g\beta. \tag{8e}$$

The governing equations (1)–(3) and (5)–(7) become

$$u_1 + u_2 + u_3 = 0 \tag{9}$$

$$u_i + \int_0^1 T_i \sin(\pi x_i \pm \alpha)\, \mathrm{d}x_i = P, \quad i = 1, 3 \tag{10}$$

$$\frac{2}{\pi}u_2 + \cos\alpha \int_0^{2/\pi} T_2 \, \mathrm{d}x_2 = P \tag{11}$$

$$u_i \frac{\mathrm{d}T_i}{\mathrm{d}x_i} = -HT_i + \lambda \frac{\mathrm{d}^2 T_i}{\mathrm{d}x_i^2}, \quad i = 1, 3 \tag{12}$$

$$H(x_i) = \begin{cases} H_0 \text{ in } \frac{1}{3} < x_i < \frac{2}{3} \\ 0 \text{ otherwise} \end{cases} \tag{13}$$

and

$$u_2 \frac{\mathrm{d}T_2}{\mathrm{d}x_2} = Q + \lambda \frac{\mathrm{d}^2 T_2}{\mathrm{d}x_2^2}. \tag{14}$$

The controlling parameters are

$$H_0 = 4h_0/d\rho cF \tag{15a}$$

$$\lambda = k/\pi^2 R^2 \rho cF \tag{15b}$$

$$Q = 4q'/\pi d^2 \rho cF\Delta T \tag{15c}$$

and α, which respectively represent the convective heat transfer in the coolers, axial conduction, the input heat flux, and the tilt angle of the loop.

BRANCH MATCHING CONDITIONS AND THE ROLE OF THERMAL CONDUCTIVITY

Energy equations (12) and (14) represent ordinary differential equations which require boundary conditions. The boundary conditions are applied at the ends of each branch of the loop, and serve to couple the velocities and temperature fields in the three branches of the loop. The matter is delicate since the order of the equations changes as axial conduction is

† F represents the friction force per unit length per unit mass flow. For laminar Poiseuille flow, $F = 32\nu/d^2$.

included or not included. The role of axial conduction, and the matching conditions at the branch junctions, are explored in this section. Whenever solutions were required, they were obtained with the aid of the symbolic manipulation program MACSYMA [15], and then verified. Numerical computations were carried out with a Hewlett Packard Integral Personal Computer.

Conducting model

When axial conduction is included, the energy equations require two boundary conditions for each branch of the loop to complete the problem specification. Continuity of fluid temperature at branch junctions A and B in Fig. 1 implies that

$$T_i = T_A, \quad i = 1, 2, 3 \qquad \text{at A} \qquad (16a)$$

$$T_i = T_B, \quad i = 1, 2, 3 \qquad \text{at B.} \qquad (16b)$$

However, T_A and T_B are unknown and two additional relations are needed. These are provided by heat balances which state that the sum of the heat fluxes arriving at A and B must vanish. The heat fluxes include convection and conduction and the part due to convection is identically zero by continuity of temperature, equations (16), and mass conservation, equation (9). Thus, the additional relations become

$$\frac{dT_1}{dx_1} + \frac{dT_2}{dx_2} + \frac{dT_3}{dx_3} = 0 \qquad (17)$$

at A and B.

Energy equations (12) and (14) can be solved in terms of T_A and T_B by using conditions (16a) and (16b). In turn, T_A and T_B can be determined from equation (17). The resulting temperature distributions in the three branches are linear/exponential functions of x_i and involve the fluid velocities in the respective branches. The continuity and momentum equations (9)–(11) form a set of four equations with the three velocities and P as the unknowns. Since the functional forms of $T_i(x_i)$ appearing therein are known, the set can be solved by using a Newton–Raphson procedure where at each iteration the Jacobian is calculated by using finite differences. Typically about ten iterations are required for solution convergence to $10^{-6}\%$.

Non-conducting model

When axial conduction is negligible, the conduction parameter λ tends to zero and most of the temperature field is governed by an outer non-conducting solution. The temperature, however, must be continuous between the outer region and an inner region (e.g. near branch junctions). The inner region is a narrow layer or zone wherein the conduction term in equation (12) is of the same magnitude as other terms in the equation. Thus, the width of this layer is of the order of λ/u_i. (Even though λ is much smaller than the other parameters in our problem, axial conduction in any branch must be included if the fluid velocity within it becomes small.) Whether or not axial boundary layers will form at a branch junction depends on the number of flows entering a junction. Axial boundary layers will form if two flows of different temperature enter a branch junction. Such axial boundary layers form only at the downstream ends of the branches which flow into a branch junction. Internal axial boundary layers also exist if the non-conducting temperature field exhibits discontinuities in its derivatives as, for instance, near the inlet and outlet to the heat exchanger. In the physical experiments to be described later, λ is about 10^{-5} times Q or H_0 (see equations (15)) and is 10^{-2} times the lowest value that can be successfully handled by our numerical solution method using the conducting model.

If the boundary layer approximation is valid we can neglect axial conduction in the outer regions of the flow by setting $\lambda = 0$ in energy equations (12) and (14). The equations are then of lower mathematical order and continuity of temperature and axial heat flux (equations (16) and (17)) cannot both be guaranteed at the branch junctions. We thus need to modify the boundary conditions for the non-conducting equations to allow for the axial boundary layers. When the axial boundary layers are thin, we need not determine the temperature distributions within the layers, since those temperature distributions contribute little to the buoyancy integrals in equations (10) and (11). The absence of conductive heat flow means that the sum of the convective fluxes at each branch junction should vanish. That is

$$u_1 T_1 + u_2 T_2 + u_3 T_3 = 0 \qquad (18)$$

at A and B. The remaining boundary condition comes from continuity of temperature at one of the two branch junctions.

Consider a branch junction with one inflowing stream and two outflowing streams. The temperatures of the two outflowing streams have to be identical and equal to that of the inflowing stream. Continuity of temperature exists at the branch junction and the mass and energy conservation equations (9) and (18) are satisfied.

On the other hand, at a branch junction with two inflowing streams and one outflowing stream the temperature may be spatially discontinuous when the two incoming streams mix. Energy equations (12) and (14) with $\lambda = 0$ can be solved for the inflowing streams in terms of the temperature at the upstream branch junction where there is temperature continuity. At the branch junction with the two inflowing streams, the outflow temperature is found by applying equation (18). We thus obtain the temperature distributions in the branches in terms of the velocities. As before, the continuity and momentum equations (9)–(11) can be solved by using a Newton–Raphson scheme.

ANALYTICAL RESULTS

The non-dimensional parameters appearing in the governing equations (9)–(15) are the tilt angle α, the

heating rate Q, the axial conduction parameter λ, and the heat transfer coefficient in the heat exchanger, H_0. The first three of these were varied; H_0 was held fixed.

The parameter ranges were selected to facilitate as much as possible a comparison with the experiments described in a subsequent section. Thus, laminar Poiseuille flow was assumed, with a friction factor $f = 64/Re$ ($Re = u_i^* d/\nu$) and a heat exchanger Nusselt number $Nu = h_0 d/k = 4$. From these relations, the friction coefficient F appearing in the governing equations is given by $32\ \nu/d^2$, and the parameter H_0 by $k/2\nu\rho c$. To obtain numerical values, the physical properties of water at 25°C were used [16]. For the dimensions of the loop described in the next section, $F = 0.30\,\mathrm{s}^{-1}$ and $H_0 = 0.08$. The non-dimensional velocities, temperature differences, and heating rates of the present section can be converted to dimensional quantities appropriate to the experiments by multiplying by $0.283\ \mathrm{m\ s}^{-1}$, 33.5°C, and 1860 W, respectively. In the case of Q, the multiplication converts a heating rate per unit length to the total heat addition in the experiment.

Effect of axial conduction

We will first investigate the effects of the axial conduction parameter, λ. The effect of axial conduction on the temperature distribution in a side branch of the loop is shown for $\alpha = 0°$ in Fig. 2(a). The abscissa is the axial coordinate x_1 or x_3. Warm fluid enters at $x = 0$ and after being cooled is discharged at $x = 1$. For $\lambda = 0$ there are abrupt changes in slope at the inlet and outlet to the heat exchanger. The effect of small values of λ is to round off the abrupt changes.

An important consideration is the effect of λ on the buoyant drive in the loop. This is displayed with a sensitivity study graphed in Fig. 2(b). The ordinate is the local change in the buoyancy force, δB, following a 5% increase in λ above a base value of 0.00015. $\delta B(x)$ represents the change in the integrand of the buoyancy integral in equation (10). The smoothing of the temperature field at the inlet and outlet to the heat exchanger causes an increase in the total buoyant force (i.e. the integral of δB is positive), and thus an increase in the fluid velocity in the loop. This is displayed in another way in Fig. 3. The solid curve is the velocity in the side branches (u_1 or u_3) for $\alpha = 0°$ as a function of λ. For small λ, the velocity approaches a constant value (corresponding to the $\lambda = 0$ limit). As λ is increased, the loop velocity increases, and peaks at about $\lambda = 0.015$. For larger λ, the loop temperature tends to become uniform (cf. Fig. 2(a)) and the velocity decreases to zero. Results for a loop tilted at $\alpha = 90°$ are shown by dashed lines in Fig. 3. For small λ, the upper side branch velocity u_1 approaches a constant value and u_3 (negative) tends to zero. For $\lambda \gtrsim 10^{-2}$, axial conduction damps out motion in the loop. This corresponds to a critical condition for the onset of motion in the loop (i.e. similar to a critical Rayleigh number).

Some notes about the solution methods are appropriate. The analytical–numerical solutions to the axially-conducting model could be obtained only for $\lambda > 10^{-5}$ due to difficulties in evaluating exponentials with large arguments. We note that λ in the physical experiments was around 5.4×10^{-7}. On the other hand, the non-conducting equations are easier to solve but the flow directions have to be guessed beforehand in order to apply the proper branch junction conditions. The directions of convective motion can be difficult to guess when multiple solutions exist. Fortunately, multiple solutions are readily found with the axially-conducting equations. Therefore, in most of the results that follow, we use a conducting model with $\lambda = 0.00015$, which could be used for all tilt angles. For small λ, the axial boundary layer regions are thin and do not significantly affect the buoyancy force. Thus, the conducting and non-conducting solutions agree for $\alpha = 0°$ in Fig. 3 as $\lambda \to 0$. Both the conducting and non-conducting methods of solution are reasonably accurate when the velocities are moderate to large. When they are small, as for u_3 at small λ in Fig. 3 for $\alpha = 90°$, it may be difficult or impossible to obtain non-conducting solutions.

The effects of tilt angle and heat input

We next examine the effects of tilt angle, α, and heat input, Q, on the flow in the loop. We will hold the non-dimensional heat transfer coefficient at $H_0 = 0.08$. We will later compare these results to experimental data and show qualitative similarities.

Velocity and temperature fields in the three branches of the thermosyphon were computed for a wide range of heat inputs. The velocities in the side branches (u_1, u_3) and the associated temperature differences across the heat exchangers ($\delta T_1, \delta T_3$) are shown in Fig. 4 for $\alpha = 0°$ and 90°. For $\alpha = 90°$ only u_1 is displayed since the flow in the other branch is nearly zero. The calculated curves represent the solution of a set of simultaneous transcendental equations. Surprisingly, the results are well described by straight lines over a two decade variation of Q. Least squares fits to the original data yield the power-law relations given in Fig. 4. The standard deviation of the power-law fits ranged from 1.1 to 2.3%. Clearly, the flow velocities for $\alpha = 90°$ are larger than for $\alpha = 0°$ (even when u_1 and u_3 for the latter are summed), and they increase more rapidly with Q. This is due to a greater mean height difference between the cooled and heated sections in the tilted geometry. Correspondingly, with the larger velocities, the δT's across the heat exchangers are smaller.

The velocities and the δT's in Fig. 4 are not independent. An overall heat balance on the loop in non-dimensional terms requires

$$\frac{2}{\pi} Q = u_1 \delta T_1 + u_3 \delta T_3 \tag{19a}$$

for a non-conducting model. The term on the left re-

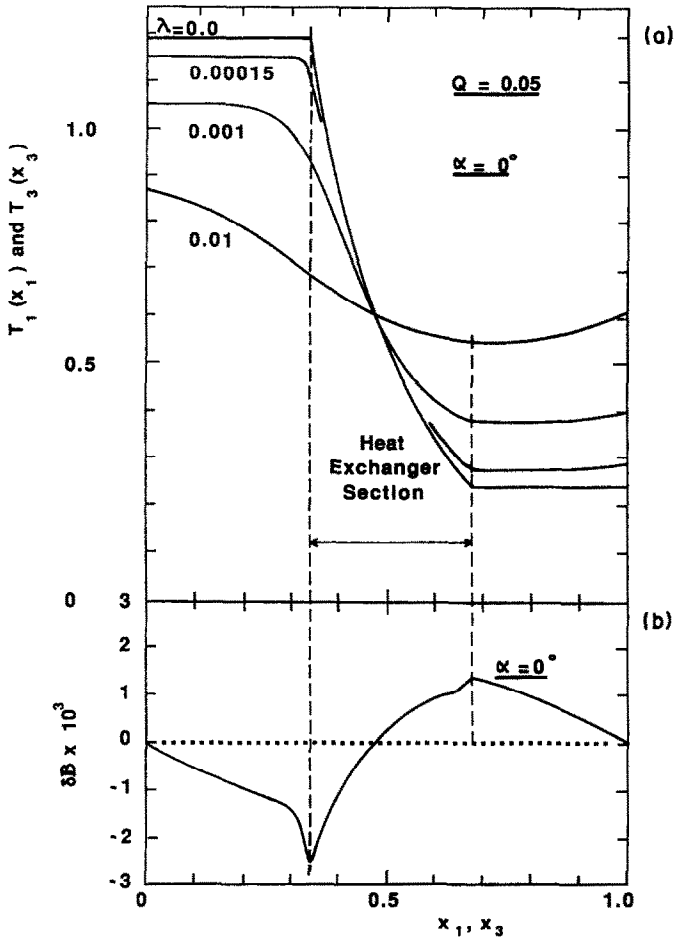

FIG. 2. (a) Effect of axial conduction parameter, λ, on the temperature distribution in a side branch of the loop: $\alpha = 0°$ and $Q = 0.05$. (b) Change in the local buoyancy force, δB, following a 5% increase in λ above a base value of 0.00015.

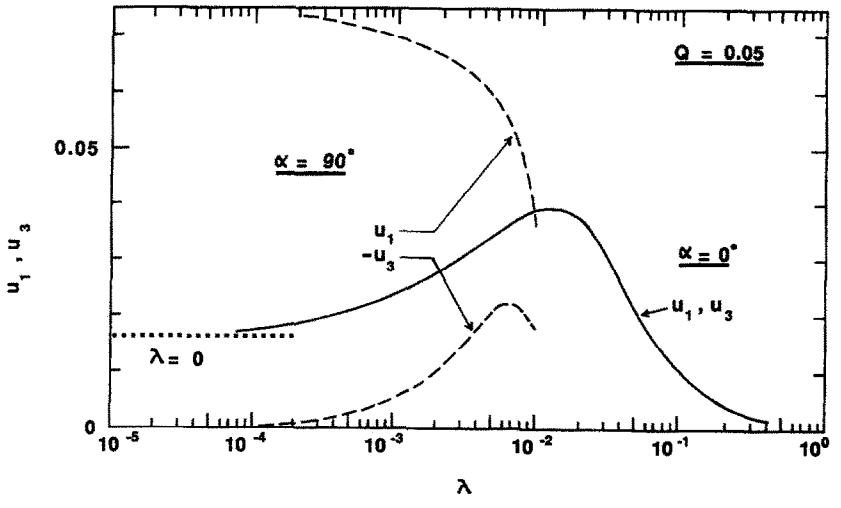

FIG. 3. Velocities u_1 and u_3 in the side branches of the loop as a function of the axial conduction parameter λ for two tilt angles: $Q = 0.05$.

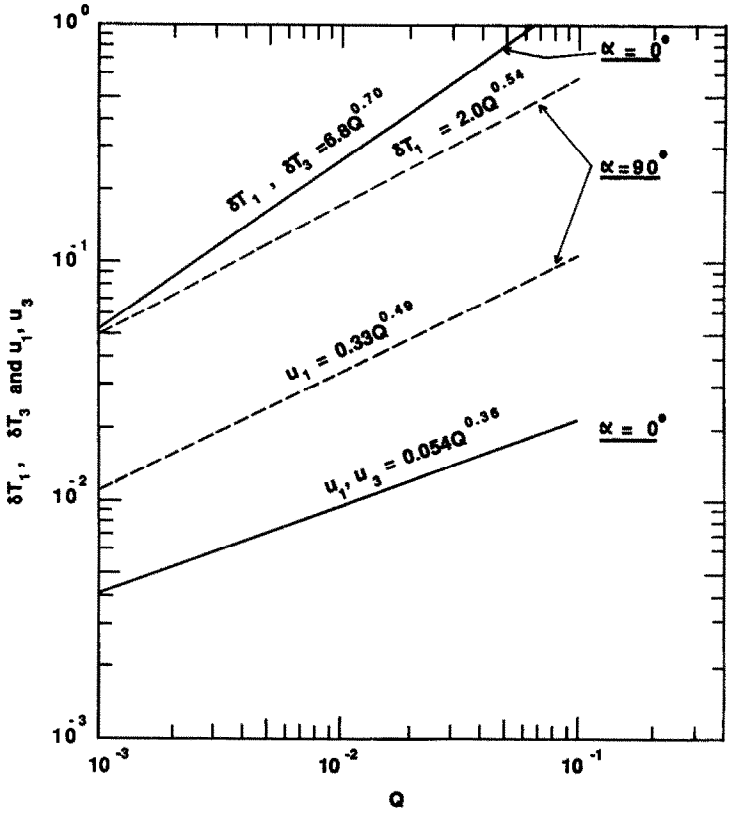

FIG. 4. Calculated side branch velocities u_1 and u_3 and temperature differences across the heat exchangers, δT_1 and δT_3, as a function of heat input Q for two tilt angles. Best-fit correlation equations are shown.

presents the heat addition to the loop, and the terms on the right represent heat removal by the side branches. For the conducting model, on the other hand

$$\frac{2}{\pi}Q = u_1\delta T_1 - \lambda\delta\left(\frac{dT_1}{dx_1}\right) + u_3\delta T_3 - \lambda\delta\left(\frac{dT_3}{dx_3}\right) \quad (19b)$$

where the effect of heat conduction is expressed in terms of differences in the slope of the temperature distribution across the coolers, $\delta(dT_i/dx_i)$. The non-zero nature of these terms is apparent from Fig. 2(a). Equations (19a) and (19b) are exactly satisfied by the non-conducting and conducting analytical solutions, respectively. Equation (19a) is only approximately satisfied by the power-law expressions for u_i and δT_i in Fig. 4. For the two values of α in Fig. 4, the appropriate exponents on Q sum approximately to unity, as required by equation (19b), but only approximately, since each least squares fit was done separately. Moreover, it is difficult to be precise about the exponent as a moderate change (say $\pm 5\%$) is just barely perceived as a change in slope in the graph.

The effect of tilt angle α on the flow in the loop is illustrated in Fig. 5. The ratio of the velocities in the two side branches of the loop, u_3/u_1, is shown in Fig. 5(a), and the ratio of the temperature differences across the two heat exchangers, $\delta T_3/\delta T_1$, in Fig. 5(b). Solid lines correspond to a heat input of $Q = 0.05$, and dashed lines to a heat input of $Q = 0.005$. In all cases, results are shown for $\lambda = 0$ and 0.00015, respectively, corresponding to non-conducting and conducting solutions.

When $\alpha = 0°$, the flows in the two side branches of the loop are equal and $u_3/u_1 = \delta T_3/\delta T_1 = 1$. As α is increased in Fig. 5(a), the velocity in the lower branch, u_3, decreases while that in the upper branch, u_1, increases. Thus, u_3/u_1 decreases. The conducting and non-conducting solutions are very close, until one of the velocities becomes small, after which the non-conducting model is unreliable. The shapes of the curves in Fig. 5(a) are generally similar at other heat inputs, although the descent is steeper at lower heat fluxes.

In Fig. 5(b), results for two heat inputs are shown. For $Q = 0.05$, the conducting and non-conducting results are in good agreement. The side branch with the lower velocity has the larger temperature drop, and $\delta T_3/\delta T_1$ exceeds unity. At larger inclinations, the lower velocity is small enough for axial conduction to become important, and the solutions for $\lambda = 0$ and 0.00015 diverge. This difference is accentuated at lower values of Q, as shown by the dashed lines. Axial conduction for both $Q = 0.05$ and 0.005 leads to reductions in the temperature difference δT_3 as α is increased. Indeed, for $Q = 0.05$, the result is a peak in $\delta T_3/\delta T_1$ at intermediate values of α, and, for $Q = 0.005$, a monotonic decay. This represents a sub-

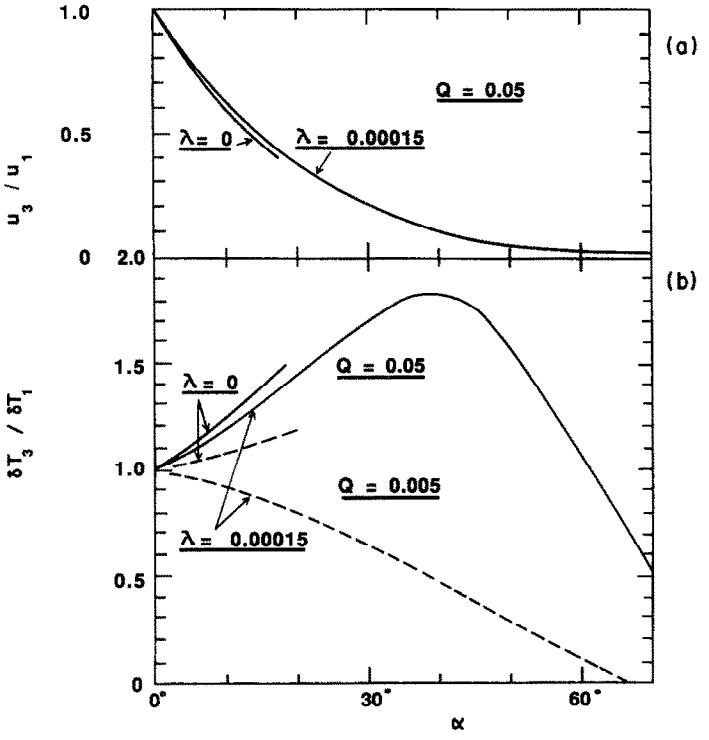

FIG. 5. (a) Ratio of calculated velocities in the side branches of the loop, u_3/u_1, as a function of tilt angle α: $Q = 0.05$. (b) Ratio of calculated temperature differences across the heat exchangers, $\delta T_3/\delta T_1$, as a function of α for $Q = 0.005$ and 0.05. Conducting ($\lambda = 0.00015$) and non-conducting ($\lambda = 0$) solutions are shown.

stantial difference in behavior for Q values differing by a factor of ten.

A flow regime diagram is presented in Fig. 6, and regions of multiple flows and flow reversals can be identified. The flow velocities u_i in the three loop branches are shown as functions of α. The heat flux and axial conduction were held constant at $Q = 0.05$ and $\lambda = 0.00015$. (The small circles represent results from the non-conducting model.) The diagram in Fig. 6 is mirror symmetric about the lines $\alpha = 0°$ and 180°.

In Fig. 6, we observe that the lower branch velocity u_3 decreases to zero as α increases from 0° to 78°. Meanwhile, the upper branch velocity u_1 increases. Beyond 78°, u_3 changes sign. We will denote this critical angle by α_c. The region near $\alpha = 90°$ reveals multiple solutions. Over a range of angles near $\alpha = 90°$, three solutions are available, each with distinct values of u_1, u_2 and u_3. In this region, the central branch of the loop is nearly horizontal with flow possible in either direction. Note that u_2 shows an s-shaped behavior. For $\alpha = 90°$, zero velocities represent a solution of the conducting equations. For clarity, portions of the u_1 and u_3 curves in this region have been omitted. (Near $\alpha = 92°$, note that the non-conducting equations show a solution (small circles) with finite velocities u_1 and u_3, while u_2 approaches zero. At $\alpha = 90°$, non-conducting solutions could not be obtained.)

Consider now the behavior near $\alpha = 90°$ in Fig. 6. If α is initially 90°, with u_1 positive, we can increase α to an angle greater than 90° without changing the direction of u_1. If α is increased beyond a maximum value, denoted by α_{max}, the flow in the upper branch will reverse and circulate in a 'natural' direction. In this case, u_1 jumps to the negative branch of the solution. The 'natural' direction is the direction in which the fluid would move if the experiment was started from rest with the given tilt angle and heat input. The angle α_{max} is graphed in Fig. 7 as a function of heat input. The zone of multiple solutions corresponds to α values between the limits given by $\alpha = 90° \pm (\alpha_{max} - 90°)$. In Fig. 7, as Q decreases to a critical value for which the rest state is marginally stable, $\alpha_{max} \to 90°$. Also, in Fig. 7, we include the critical angle α_c which denotes the angle at which the flow in the lower side branch, u_3, changes direction. Near $\alpha = \alpha_c$, increasing Q favors positive motion in branch 3, requiring thus an increase in tilt angle for the flow to change direction.

EXPERIMENTAL OBSERVATIONS

The analytical solutions can be compared with observations on a laboratory double-loop thermosyphon. The apparatus and experimental results are described in this section.

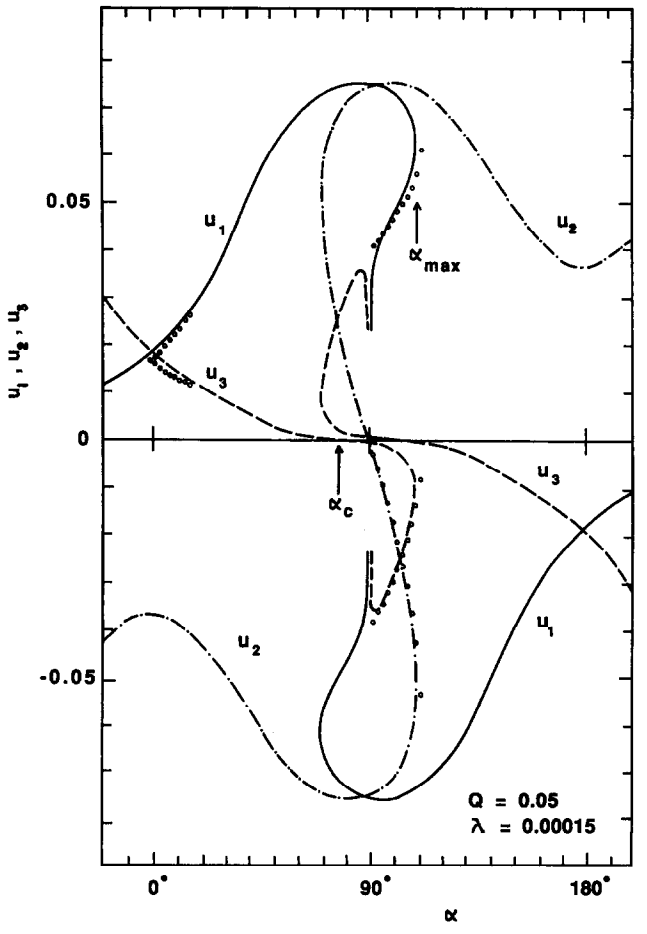

FIG. 6. Calculated velocities u_1, u_2 and u_3 in the three branches of the loop as a function of tilt angle α: $Q = 0.05$ and $\lambda = 0.00015$. Non-conducting solutions ($\lambda = 0$) are shown with small circles. α_{max} denotes the angle at which the calculated velocity u_1 in the upper side branch of the loop reverses direction. α_c denotes the angle at which the velocity u_3 in the lower side branch reverses direction.

Apparatus

The experimental loop is in the form of a glass torus with a straight glass tube connecting the outer loop along its diameter (see Fig. 1). The loop has a tube inner diameter of $d = 9.75$ mm and a torus radius of $R = 300$ mm. An electrical resistance heater (34.8 Ω) is wound over the entire length of the center branch, and is supplied with alternating current from a variable transformer. External glass heat exchangers were built over the middle thirds of the side branches. Tap water is circulated through the heat exchangers to provide cooling. To allow for flow visualization and velocity measurements, no attempt was made to insulate the loop. The whole loop can be tilted about its horizontal axis and the tilt angle measured to half a degree by a pointer and protractor.

The temperature of the cooling water was about 20°C and constant to within 0.2°C for any run. The cooling water flow rate was around 115 ml s^{-1} for each heat exchanger, which was high enough so that the temperature increase of the cooling water was less than 0.2°C. Through small holes in the walls of the glass loop, 36 gage (0.127 mm diameter) copper–constantan thermocouples were inserted. Temperatures inside the loop were measured at the inlet and outlet to the heat exchangers as well as at the two branch junctions. Although the thermocouples were located near the duct centerlines, the measured temperatures are likely to be reasonably close to the bulk temperatures due to the expected flatness of the transverse temperature profiles at the measurement stations. Thermocouple voltages were measured with a Hewlett Packard 3466A Digital Multimeter and were also recorded on a Houston Instrument pen recorder.

Fluid velocities in the side branches of the loop were obtained from flow visualization. Small fibers of colored yarn were used as tracers, and their advance was manually chronometered. These fibers can be assumed to move with the flow since they have a settling velocity of less than 1 cm min^{-1} in stagnant water. The velocity in the center branch could not be measured since it was obscured by the electrical heater. There was a noticeable velocity profile across the diameter d of the thermosyphon tube. However, only the velocities of the tracers closest to the duct centerline were measured. With this selection, the scat-

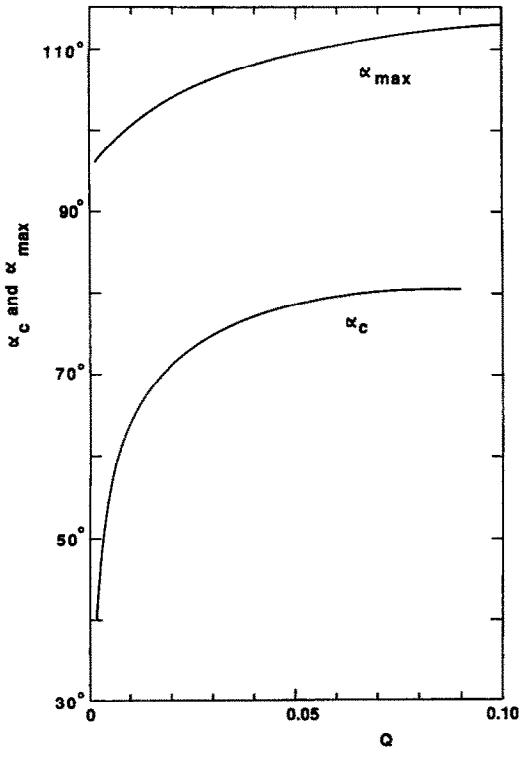

FIG. 7. Calculated values of α_{max} and α_c as a function of heat input Q: $\lambda = 0.00015$.

ter in the velocity measurements was roughly $\pm 5\%$ about a mean value. On the basis of a heat balance at the heater, the bulk average velocity was estimated to be about 0.54 of the tracer velocity. This is consistent with a Poiseuille-like velocity profile, in which bulk and centerline velocities are in the ratio 1 : 2.

Steady state was reached within 15 min after turning the heater on. Measurements were taken 30 min or more after a change of input heat flux or tilt angle. At all heat fluxes, even though the temperature of the fluid in the entire loop fluctuated in phase with an amplitude of 1–1.5°C and with a period of about 20 min, the temperature differences were almost steady. For example, the temperature differences δT_1 and δT_3 were found to fluctuate about 1.5% around their mean values.

The graphical results in the next section have non-dimensional axes, and some have additional dimensional axes. The appropriate conversion factors were given at the start of the preceding analytical results section. However, only a qualitative comparison between experiment and analysis is possible. The experiments provide point measurements of temperature and velocity. The analytical results, on the other hand, are expressed in terms of bulk fluid temperature and mean duct velocity. An additional factor in the experiments is heat transfer to and from the room. In one heat balance test, about 82% of the heat taken out at the coolers came from the heaters, the rest being from the room. Nevertheless, even with the foregoing reservations, it will be apparent that the agreement between experiment and analysis is favorable.

Experimental results

The experimental results are presented in a manner which parallels the analytical results of the previous section. Indeed, Figs. 8–11 of this section may be compared directly with Figs. 4–7 of the previous section. Again, as noted earlier, precise quantitative comparisons are not possible.

Experiments were carried out for a range of heating rates, Q. The measured mean centerline velocities in the side branches of the loop (u_1, u_3), and the temperature differences $(\delta T_1, \delta T_3)$, are shown in Fig. 8 for $\alpha = 0°$ and 90°. For $\alpha = 0°$, the velocities in the side branches differed by less than 7%, and the temperature differences by less than 5%, and averages of the two branches were taken. For $\alpha = 90°$, only u_1 and δT_1 for the upper side branch were measured and are shown. The velocity u_1 is much larger than for $\alpha = 0°$ and measurements were more difficult. Also, $\alpha = 90°$ falls in the range $\alpha_c < \alpha < \alpha_{max}$. Thus, the u_3 velocities were small and negative, and there was a very slow movement of fluid toward the hot branch junction. From the agitated motion of the tracers in the outflow from this junction, there was a vigorous mixing of the incoming hot stream from the central branch and the incoming cold stream from the lower branch.

Power-law correlations of the experimental data are also given in Fig. 8. Omitting the data at the lowest heat flux, the velocities correlate with a standard deviation of 4%, and the temperature differences correlate to within 3%. The correlations are generally similar to the theoretical correlations in Fig. 4. Indeed, the velocity correlations in Figs. 8 and 4 differ in magnitude by a factor of about two, corresponding roughly to the difference between centerline and bulk velocities in laminar duct flow. The largest differences in the correlations occur for the temperature difference δT_1 for $\alpha = 90°$. The experiments show a weaker power law dependence on Q than do the analytical results. For each value of α in Fig. 8, the exponents on Q sum approximately to unity as required by the heat balance, equation (19a) or (19b). These equations represent a basic balance, independent of other equations and assumptions, but with coefficients that depend on simplifications made in the theory.

The influence of tilt angle α on the ratio of the velocities in the two side branches of the loop, u_3/u_1, and the ratio of the temperature differences, $\delta T_3/\delta T_1$, is shown in Figs. 9(a) and (b), respectively. Solid lines correspond to $Q = 0.112$ and the dashed lines to $Q = 0.014$. The trends in Fig. 9 can be compared to Fig. 5. As with the analytical solutions, the shape of the experimental curve for u_3/u_1 in Fig. 9(a) is maintained at other heat fluxes, but the curve gets steeper as Q is reduced. Other than the fact that the experimental curve for $\delta T_3/\delta T_1$ at $Q = 0.014$ seems to have a second maximum, the general shapes of the

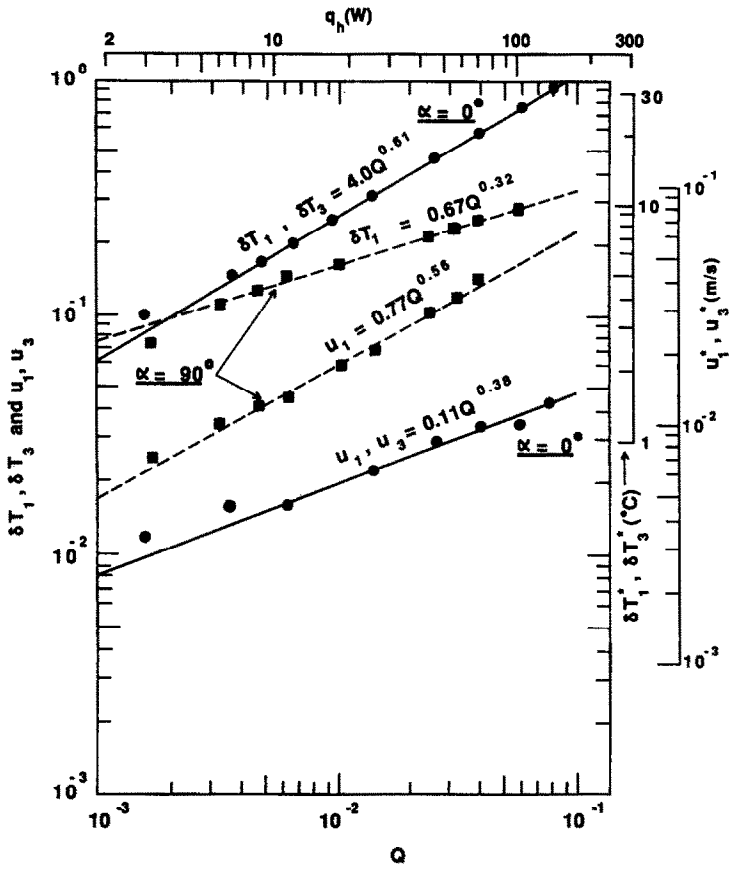

FIG. 8. Experimentally-measured side branch velocities u_1 and u_3 and temperature differences across the heat exchangers, δT_1 and δT_3, vs the heat input Q for two tilt angles. Best-fit correlation equations are shown. Dimensional axes are shown at the top and right sides.

curves in Fig. 9(b) are in qualitative accord with those in Fig. 5(b). The experimental results for $\delta T_3/\delta T_1$ thus confirm that axial conduction or equivalent effects like heat conduction through the glass or fluid mixing become important at low velocities (i.e. when u_3 decreases as α increases) or at lower heat fluxes.

Velocity measurements in the two side branches of the loop are shown as a function of the tilt angle, α, in Fig. 10. The heat input was held constant. The velocity u_3 becomes small and difficult to measure as α is increased. Temperature measurements indicate that u_3 reverses direction at $\alpha = 75°$. This value is close to the analytical value of α_c in Fig. 7. The velocity in the upper branch, u_1, increases many times on tilting the loop and reaches a maximum before 90°, similar to the analytical prediction in Fig. 6.

The range of angles for which multiple steady states are observed is shown in Fig. 11. Note that two different Q scales (above and below) are used. Multiple steady states occur over the range of tilt angles bounded by $\alpha = 90° \pm (\alpha_{max} - 90°)$. Both clockwise and counterclockwise flows were observed in this range of α. Figure 11 corresponds to Fig. 7 of the analysis. In the experiments, the inclination angle was progressively increased by 0.5°, with Q held constant, until a catastrophic change from 'anti-natural' to 'natural' flow occurred. Thus, α_{max} represents the largest value of α for which a flow reversal did not take place. At the lower heat fluxes it was necessary to wait more than 15 min for the change. The qualitative nature of α_{max} in Figs. 7 and 11 is different. The reason is that the present steady-state theory deals only with the existence of solutions, and not with their stability. Thus, the theoretical curve in Fig. 7 is an existence limit. However, in a region with multiple steady states, those flows which are unstable will not be observed. It is possible that the experimental results in Fig. 11 represent the observed stability limit. Except at the very lowest values of Q, the observed values of α_{max} are smaller than the theoretical existence limit, and this difference increases as Q increases. For very small heat fluxes the measured α_{max} should go to 90°. This was not observed.

The critical angle α_c for flow reversal in the lower branch was also measured. The tilt angle was decreased in 0.5° increments from $\alpha = 90°$ until the flow in the lower leg changed direction. This was indicated by a change in sign of the temperature

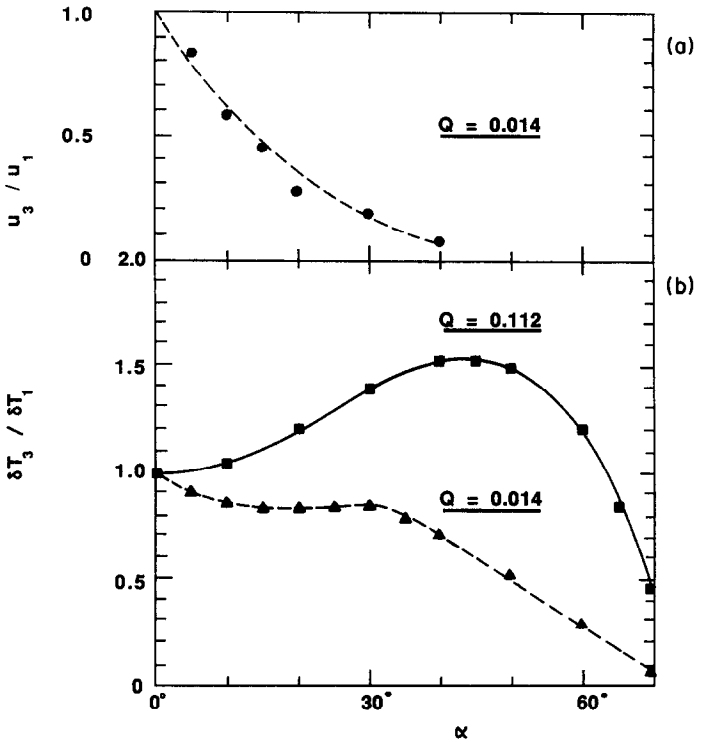

FIG. 9. (a) Ratio of experimentally-measured velocities in the side branches of the loop, u_3/u_1, as a function of tilt angle α: $Q = 0.014$. (b) Ratio of experimentally-measured temperature differences across the heat exchangers, $\delta T_3/\delta T_1$, as a function of α for $Q = 0.014$ and 0.112.

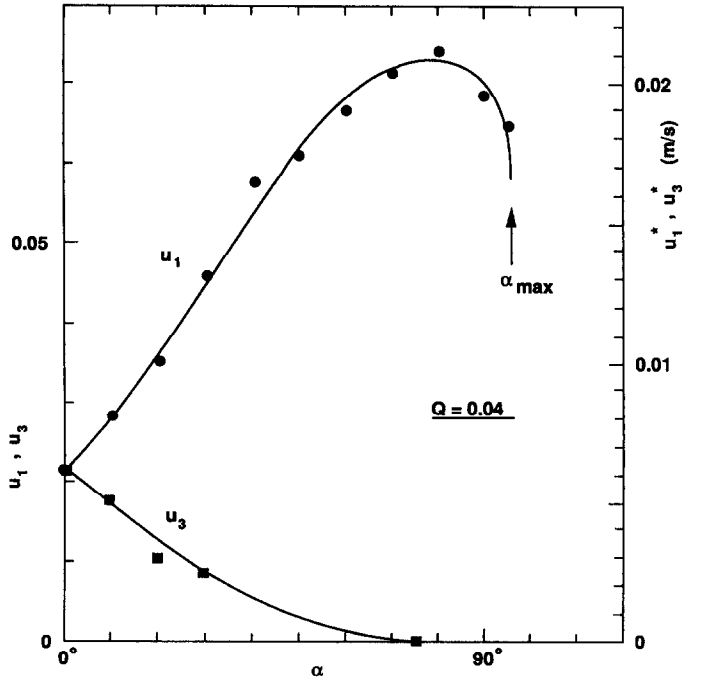

FIG. 10. Experimentally-measured velocities u_1 and u_3 in the two side branches of the loop as a function of tilt angle α: $Q = 0.014$.

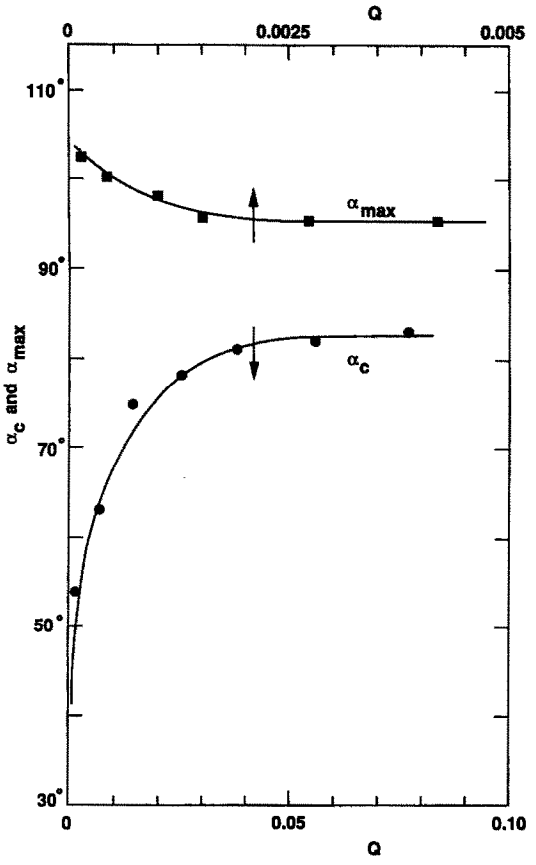

FIG. 11. Experimentally-measured values of α_{max} and α_c as a function of Q. α_{max} denotes the tilt angle at which the velocity u_1 in the upper side branch of the loop was observed to reverse direction. α_c denotes the tilt angle at which the velocity u_3 in the lower side branch was observed to reverse direction.

difference across the lower heat exchanger as measured by a differential thermocouple connected across the heat exchanger. The variation of α_c with Q is shown in Fig. 11, and closely follows the analytical result in Fig. 7.

CONCLUSIONS

Multiple-loop thermosyphons can be modeled one-dimensionally with or without axial conduction. With axial conduction, the continuity of temperature and heat flux at branch junctions is guaranteed. Without axial conduction, the continuity of temperature cannot be assured. At large fluid velocities, the temperature adjustment region near a branch junction is confined to a narrow axial thermal boundary layer. Outside of this boundary layer, the non-conducting energy equations can be applied if a suitable heat balance boundary condition is used at the downstream end of each branch. If the fluid velocity is small, as happens in the lower branch of the present loop at large tilt angles, the effect of axial conduction is spread over a larger region and must be taken into account as it affects the buoyancy of the fluid in the branch.

The comparison between theory and experiment reveals strong qualitative, and almost quantitative, agreement. This is encouraging in view of the limitations of theory and experiment. The analytical approximations include one-dimensionality and constant friction and heat transfer coefficients. In the experiments, only point velocities and temperatures could be measured (approximately at the duct centerline), and not mean or bulk values. Also, the adiabatic sections of the loop were not truly adiabatic.

Natural convection loops which show symmetry of both heating and cooling about a vertical plane (the present loop for $\alpha = 90°$), such that a rest state is theoretically possible, can have multiple steady states for small tilt angles about the symmetry plane. This was confirmed in the present case and was previously observed in a square single-loop thermosyphon [17].

Prior work suggests that axial conduction might only be significant near the onset of motion from a rest state in natural convection systems [13]. As we have shown in Figs. 5 and 9, axial conduction can be important when flow velocities are small, but nonzero. Thus, the decision to neglect axial conduction in an analysis must be carefully considered.

On tilting the central branch from a vertical position ($\alpha = 0°$ in the present thermosyphon), a difference between the two side branches is imposed. Flow in the lower branch decreases significantly while that in the upper branch increases. For $\alpha = 10°$, the velocities in the two branches differ by more than 40%. This points out the sensitivity of the flow in a multiple-loop thermosyphon to differences between branches that might have been designed to be identical, but in practice might not be. Large differences in symmetry can lead to essentially stagnant flow in one of the branches.

Acknowledgements—We thank Filiberto Gutiérrez and the Instituto de Ingeniería of the Universidad Nacional Autónoma de México in Mexico City for fabricating the experimental loop. The loop was assembled and instrumented at Cornell University. The research was sponsored in part by the National Science Foundation under Grant MEA-8401489 while one of the authors (M.S.) was at Cornell University on leave from the Universidad Nacional Autónoma de México.

REFERENCES

1. Y. Zvirin, A review of natural circulation loops in pressurized water reactors and other systems, *Nucl. Engng Des.* **67**, 203–225 (1981).
2. A. Mertol and R. Greif, A review of natural circulation loops. In *Natural Convection: Fundamentals and Applications* (Edited by W. Aung, S. Kakac and R. Viskanta), pp. 1033–1071. Hemisphere, New York (1985).
3. A. S. Lavine, R. Greif and J. A. C. Humphrey, Three-dimensional analysis of natural convection in a toroidal loop: effect of tilt angle, *J. Heat Transfer* **108**, 796–805 (1986).
4. P. S. Damerell and R. J. Schoenhals, Flow in a toroidal

thermosyphon with angular displacement of heated and cooled sections, *J. Heat Transfer* **101,** 672–676 (1979).
5. T. E. Britt and D. C. Wood, Free convection in a partially submerged fluid loop, ASME Paper 83-HT-67 (1983).
6. A. N. Opanasenko, V. M. Selivanov and N. N. Shan'gin, Thermal stratification of reactor coolant under steady state and transient nuclear power plant operating conditions, *Heat Transfer—Soviet Res.* **15,** 132–140 (1983).
7. J. C. Chato, Natural convection flows in parallel-channel systems, *J. Heat Transfer* **85,** 339–345 (1963).
8. Y. Zvirin, P. R. Jeuck III, C. W. Sullivan and R. B. Duffey, Experimental and analytical investigation of a natural circulation system with parallel loops, *J. Heat Transfer* **103,** 645–652 (1981).
9. Y. Zvirin and Y. Rabinovitz, On the behavior of natural circulation loops with parallel channels, *Proc. 7th Int. Heat Transfer Conf.*, Munich, F.R.G., Vol. 2, pp. 299–304 (1982).
10. Y. Zvirin, The onset of flows and instabilities in a thermosyphon with parallel loops, *Nucl. Engng Des.* **92,** 217–226 (1986).
11. Y. Zvirin, Natural circulation loops with parallel channels—transient behavior, *Nucl. Engng Des.* **84,** 73–81 (1985).
12. M. Sen and J. L. Fernández, One-dimensional modeling of multiple loop thermosyphons, *Int. J. Heat Mass Transfer* **28,** 1788–1790 (1985).
13. Y. Zvirin, The onset of motion in a toroidal thermosyphon, *J. Engng Math.* **20,** 3–20 (1986).
14. J. Kevorkian and J. D. Cole, *Perturbation Methods in Applied Mathematics*. Springer, New York (1981).
15. R. H. Rand, *Computer Algebra in Applied Mathematics: an Introduction to MACSYMA*. Pitman, Boston (1984).
16. G. K. Batchelor, *An Introduction to Fluid Dynamics*. Cambridge University Press, London (1967).
17. R. Acosta, M. Sen and E. Ramos, Single-phase natural circulation in a tilted square loop, *Wärme- und Stoffübertr.* **21,** 269–275 (1987).

ETUDE ANALYTIQUE ET EXPERIMENTALE DE LA CONVECTION PERMANENTE DANS UN THERMOSIPHON A DOUBLE BOUCLE

Résumé—On étudie la convection naturelle permanente dans une boucle toroïdale avec une branche diamétrale chauffée et des branches latérales froides. La boucle est tournée pour faire varier l'angle d'inclinaison de la branche diamétrale. Une analyse monodimensionnelle donne les distributions de vitesse et de température dans la boucle. Les effets de la conduction axiale sont examinés. Quand l'inclinaison depuis la verticale augmente, le fluide dans la branche basse diminue et se renverse. L'écoulement à travers la branche centrale augmente et le principal chemin de retour est à travers le coté supérieur de la branche. Pour des petites inclinaisons autour de l'horizontale, il existe plusieurs états stationnaires. Des expériences comparatives sur une boucle de verre remplie d'eau sont en accord qualitatif avec l'analyse et on observe de multiples états stationnaires.

ANALYTISCHE UND EXPERIMENTELLE UNTERSUCHUNG DER STATIONÄREN KONVEKTION IN EINEM DOPPELTEN THERMOSYPHON-LOOP

Zusammenfassung—Die stationäre natürliche Konvektion in einem Torus mit einem zentralen beheizten Teil und zwei gekühlten Seitenteilen wird untersucht. Der Kreislauf wird zur Veränderung des Neigungswinkels des beheizten Teils gedreht. Eine eindimensionale Analyse liefert die Fluidgeschwindigkeiten und die Temperaturverteilungen im Kreislauf. Die Einflüsse der axialen Leitung werden untersucht. Mit zunehmendem Neigungswinkel zur Vertikalen wird die Strömung im unteren Teil langsamer und ändert dann ihre Richtung. Die Strömung durch den mittleren Teil nimmt zu und der Hauptrückstrom führt durch den oberen Teil. Für kleine Neigungswinkel nahe der Horizontalen gibt es mehrfache stationäre Zustände. Vergleichende Experimente mit einem wassergefüllten Glaskreislauf stimmen qualitativ mit der Analyse überein, und es werden mehrfache stationäre Zustände beobachtet.

АНАЛИТИЧЕСКОЕ И ЭКСПЕРИМЕНТАЛЬНОЕ ИССЛЕДОВАНИЕ УСТАНОВИВШЕЙСЯ КОНВЕКЦИИ В ТЕРМОСИФОНЕ С ДВОЙНЫМ КОНТУРОМ

Аннотация—Исследуется установившаяся естественная конвекция в тороидальном контуре с нагреваемым диаметральным и охлаждаемыми боковыми отводами. Контур поворачивается для изменения угла наклона диаметрального отвода. С помощью одномерного анализа получены распределения скорости и температуры в контуре. Исследуются эффекты аксиальной передачи тепла. С увеличением угла отклонения от вертикали течение жидкости в нижнем боковом отводе замедляется, а затем изменяется на обратное. Течение в центральном отводе ускоряется, и обратное течение происходит в основном через верхний отвод. При небольших углах наклона к горизонтали отмечаются целый ряд стационарных состояний. Результаты анализа качественно согласуются с экспериментальными данными, полученными в стеклянном заполненном водой контуре, где также наблюдается неединственное стационарное состояние.